

Cell-Free Massive MIMO Under Mobility: A Fairness-Differentiated Handover Scheme

Yunlu Xiao, Marina Petrova, and Ljiljana Simić

Abstract—While cell-free massive MIMO (CF-mMIMO) offers both uniform and high network-wide throughput in static networks, its performance in a mobile network is not yet fully addressed. In this paper, we evaluate the performance of a mobile CF-mMIMO network under a comprehensive throughput model and show that it suffers from large performance degradation due to the combined effect of channel aging and handover delay. To improve the performance of CF-mMIMO under mobility, we propose a fairness-differentiated handover scheme. Our scheme differentiates the handover policy for different users by their channel conditions compared to a threshold based on Jain’s fairness index, in order to prioritize handovers for the poorly-served users. We present an extensive evaluation of the mobile throughput performance of our handover scheme with realistic urban network distributions and UE mobility patterns. Our results show that our scheme significantly outperforms the existing literature benchmarks when considering both channel aging and handover delay cost. Importantly, the advantage of UE-centric over network-centric CF-mMIMO, of uniformly good performance over the network, is uniquely preserved under mobility by our handover scheme. We thus show that CF-mMIMO can be a feasible architecture for practical mobile networks.

Index Terms—cell-free massive MIMO, mobility performance, handover scheme, channel aging

I. INTRODUCTION

CELL-free massive multiple-input-multiple-output (CF-mMIMO) has been proposed [2] to satisfy the requirements of ubiquitous connectivity in future networks by providing both high and uniform throughput performance through the whole communication network by coordinating all access points (APs) to jointly serve all users (UEs). Unlike the traditional cellular network, where one base station only serves UEs within its cell, CF-mMIMO coordinates all APs in the network to serve a given UE. This architecture thereby combines the high throughput benefit of massive MIMO and the uniform throughput benefit of distributed MIMO [3]. With no cell boundaries nor changes in serving APs, the CF-mMIMO network thus eliminates the cell-edge effect and handover problems to provide significantly better and more uniform performance over the network [4]. However, in practical networks, coordinating all APs to simultaneously serve all UEs brings very high signal processing and system overhead. Scalable CF-mMIMO is thus proposed [5] to limit the system cost by managing the APs via several disjoint CPU clusters

and serving a given UE with a finite cluster set. The UE first selects a few APs that have the best channel conditions, and is then served by the disjoint CPU clusters that those APs belong to [6]. Different from the network-centric distributed MIMO, i.e., the coordinated multipoint with joint transmission (CoMP-JT), where the UE is only served by the CPU cluster it resides in [7, 8], this UE-centric architecture effectively forms a serving AP set that surrounds the UE, and thus reduces the cluster-edge effect and achieves higher throughput compared to the network-centric distributed MIMO architecture.

In case of UE mobility, the CF-mMIMO architecture is affected by both channel aging and handover. Firstly, the serving AP set selection and signal processing of CF-mMIMO depend on channel information, which is quickly outdated due to a fast-changing mobile channel, i.e., the channel aging effect [9]. Furthermore, maintaining a UE-centric serving AP set for a mobile UE requires frequent changes of the serving APs, leading to high handover rates [10]. This raises the question of whether CF-mMIMO would maintain its high and uniform throughput performance under mobility.

The prior literature studies channel aging and handover separately. The channel aging effect for CF-mMIMO is modelled in [9] to present the throughput degradation of original CF-mMIMO under mobility. Channel aging for scalable UE-centric CF-mMIMO is furthermore studied in [11], showing the great impact of channel aging on throughput under high mobility. To improve the throughput under channel aging, a finite impulse response Wiener predictor is proposed in [12] and the duration of the communication block is optimized in [13]. The results showed that although the throughput of UE-centric CF-mMIMO decreases under channel aging, it is still better than the traditional network-centric distributed MIMO architecture. However, these studies consider solely the channel aging effect and entirely neglect handover analysis, and thus their mobility model is incomplete and the drawn conclusions are biased. Although handover is a well-studied topic in cellular networks [14], the handover model and scheme for the CF-mMIMO architecture have been seldom investigated. We modelled handover as a delay cost in [10] and showed that without channel aging, the UE-centric CF-mMIMO architecture achieves higher throughput for moderate mobility levels than network-centric. However, we showed in [15] that when both channel aging and handover are considered, the combined mobility impact brings significant throughput degradation to UE-centric CF-mMIMO, in fact rendering it unattractive compared to a network-centric architecture without a smart, selective handover strategy in place.

Several handover schemes for CF-mMIMO have been pro-

The authors are with the Institute of Networked Systems, while M. Petrova is also with the Mobile Communications and Computing Teaching and Research Area at RWTH Aachen University, Aachen 52072, Germany (email: yxi@inets.rwth-aachen.de, petrova@mcc.rwth-aachen.de, lsi@inets.rwth-aachen.de). The preliminary conference version of this work [1] was presented at IEEE WCNC 2024, Dubai.

posed in [16–19]. A UE-performance-aware handover scheme is proposed in [16] to only trigger the handover of a given UE when its performance has fallen by a certain margin. The hysteresis scheme in [18] additionally requires that the performance after handover is better than before handover by a certain margin. A machine-learning-based scheme is derived in [19] by modeling the handover as a partially observable Markov decision process. However, the performance of these schemes is chiefly evaluated in terms of their success in reducing the handover rate. For the throughput evaluation, [17, 18] neglect mobility costs entirely and [16, 19] solely consider the channel aging effect, neglecting the handover delay overhead. Therefore, it is not clear whether the existing benchmark handover schemes can indeed provide high and uniform throughput for CF-mMIMO under mobility when both channel aging and handover are considered. In this paper, we re-evaluate the benchmark schemes [16–18] using a comprehensive throughput model that considers both channel aging and handover delay costs. We show that they in fact fail to provide uniformly good performance across the network, due to reducing the UE handover rate of CF-mMIMO indiscriminately by applying the same handover policy for all UEs. Therefore, the handover schemes from the prior literature fail to make CF-mMIMO a viable architecture under mobility.

To address this, in this paper we propose a *fairness-differentiated* handover scheme to significantly improve the performance of CF-mMIMO and for the first time make CF-mMIMO a feasible architectural concept for mobile networks. We employ Jain’s fairness index to evaluate whether the UE is fairly served in terms of serving AP set assignment and channel conditions. We set a handover-policy-differentiation threshold for the UE performance, based on the fairness index, and apply different handover policies to the UEs above or below the threshold, thus prioritizing handovers for the poorly-served UEs.

We conduct a performance evaluation of our proposed scheme under both the scenario of randomly uniformly distributed APs and the random way point (RWP) UE mobility model, which is widely adopted in the prior work [9–13, 15, 16, 18, 19], as well as the scenario of realistic urban network distributions and mobility patterns. In a realistic urban network, the locations of APs and UEs are constrained by buildings, streets, and public squares, e.g., an AP cannot be placed in the middle of a street and a UE cannot walk through the building walls. Therefore, the realistic AP distribution and UE mobility patterns are likely to be highly non-uniform and cannot be well modelled by the widely assumed random uniform distribution and mobility pattern. Consequently, it is not yet clear whether the performance of mobile CF-mMIMO observed in random uniform networks still holds in realistic urban networks. To the best of our knowledge, the handover and mobility management problem of CF-mMIMO in practical scenarios has been rarely studied. A realistic urban topology of the city area of Seoul is considered in [17], but with RWP UE mobility. Both a realistic topology and mobility pattern are assumed in [20], but without any handover analysis.

In this paper, we show that under the comprehensive mobility throughput model, our proposed handover scheme

significantly outperforms the existing schemes and restores the throughput advantage of CF-mMIMO against the traditional network-centric architecture, not only in the scenario of randomly uniformly distributed APs and RWP UE mobility, but also in realistic urban networks. We thus make CF-mMIMO an attractive architecture for not only static but also practical mobile networks.

Our key contributions are:

- We present a comprehensive study of mobile CF-mMIMO using a throughput model that considers both channel aging and handover overheads. We show that under this model, the performance of CF-mMIMO suffers heavily due to fast changing serving AP sets, and thus is no longer attractive for mobile networks compared to CoMP-JT without a smart handover scheme. The existing benchmark handover schemes are also shown to perform poorly under mobility due to indiscriminately reducing the handover rate of all UEs.
- We propose a novel *fairness-differentiated* handover scheme that significantly improves the throughput of mobile UEs in CF-mMIMO networks. Our results show that our handover scheme significantly outperforms the existing benchmarks. We specifically compare the performance of the handover schemes under UE-centric CF-mMIMO and CoMP-JT, showing that our scheme uniquely allows UE-centric CF-mMIMO to maintain its advantage over network-centric CoMP-JT under mobility.
- We conduct an extensive performance evaluation of the handover schemes in different urban network distributions and UE mobility patterns in realistic city layouts and show that our proposed scheme achieves superior throughput among all considered scenarios, especially for the poorly-served UEs. Importantly, we thus propose for the first time a handover scheme that delivers in practice the promise of CF-mMIMO of high and uniform performance, for not only static but also mobile networks.

The rest of the paper is organized as follows. Sec. II presents our system model. Sec. III details our proposed handover algorithm design and the prior benchmark handover schemes. Sec. IV details the simulation scenarios. Sec. V presents our results and Sec. VI concludes the paper. The related work is summarized in Table I.

II. SYSTEM MODEL

A. Network Architecture

We consider a mobile network with M static APs and K mobile UEs located in an area S , all with a single antenna. The APs are distributed as a Poisson Point Process (PPP) distribution of density $\lambda = M/S$. We assume the UEs are initially distributed as PPP of density $\lambda_U = K/S$ and model their movement with the random way point (RWP) model. To study the performance of mobile CF-mMIMO in realistic urban network layouts, we also consider site-specific locations of APs and mobility patterns of UEs as detailed in Sec. IV.

We consider two CF-mMIMO network architectures to form the serving AP set for a given UE: the *UE-centric* architecture, which is the scalable version of the original CF-mMIMO [6], and the *network-centric* architecture, which is in fact

TABLE I
RELATED WORK ON MOBILITY MANAGEMENT FOR CF-mMIMO.

Reference studies	Network architecture UE-centric network-centric	Handover scheme	Handover delay cost	Channel aging	Practical topology	Realistic mobility pattern
[9]	unscalable CF-mMIMO	✗	✗	✓	✗	✗
[10]	✓	✓	✗	✓	✗	✗
[11]	✓	✗	✗	✓	✗	✗
[12, 13]	massive MIMO	✗	✗	✓	✗	✗
[15]	✓	✓	✗	✓	✗	✗
[16]	✓	✗	UE-performance-aware	✗	✗	✗
[17]	✓	✗	UE-performance-aware	✗	✓	✗
[18]	✓	✗	Hysteresis	✗	✗	✗
[19]	✓	✗	Partially observable Markov decision process	✗	✓	✗
[20]	✓	✗	✗	✓	✓	✓
This paper	✓	✓	Fairness-differentiated	✓	✓	✓

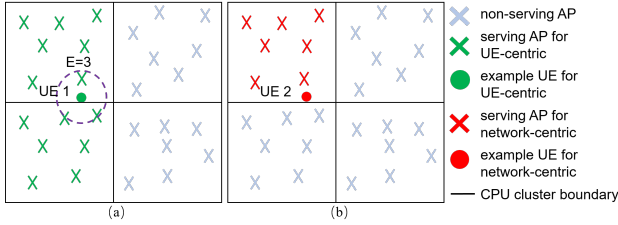


Fig. 1. CF-mMIMO architectures: (a) UE-centric and (b) network-centric.

CoMP-JT [8]. The architectures are illustrated in Fig. 1. For the UE-centric CF-mMIMO architecture, the APs are assigned to disjoint CPU clusters. In Fig. 1, the example UE 1 first selects E APs with the best channel condition, and is then served by all APs in the clusters that these E APs belong. The APs in one CPU cluster connect to the CPU via fronthaul links, while all CPUs connect to the core network via backhaul. We define the set of APs that are in the same CPU cluster as AP m as \mathbf{Q}_m . The average size of \mathbf{Q}_m , $Q = |\mathbf{Q}_m|$, is then the average number of APs in one CPU cluster, i.e., the CPU cluster size. The CPU performs the centralized signal processing, AP selection, and handover decisions (*cf.* Sec. II-B) for the APs and UEs residing in its cluster. The example UE 2 forms the serving AP set as per network-centric CF-mMIMO. In the network-centric architecture, APs are also assigned to disjoint CPU clusters and the UE is served by the APs in the CPU cluster it resides in; network-centric CF-mMIMO is thus a special case of UE-centric with $E = 1$.

B. Channel Model & Signal Processing

We assume a three-slope log-distance path loss channel model [2], which gives the path loss with shadowing between AP m and UE k as $L_{mk}[t] = \bar{L}_{mk}[t]10^{\sigma z_{mk}/10}$, with σ as the shadowing deviation, $z_{mk} \sim N(0, 1)$, and the average path loss in dB as:

$$\bar{L}_{mk} = \begin{cases} L_0 + 35 \log_{10}(d_{mk}[t]), & d_{mk}[t] > d_c \\ L_0 + 15 \log_{10}(d_c) + 20 \log_{10}(d_0), & d_{mk}[t] \leq d_0, \\ L_0 + 15 \log_{10}(d_c) + 20 \log_{10}(d_{mk}[t]), & \text{otherwise} \end{cases} \quad (1)$$

where $d_{mk}[t]$ is the distance between AP m and UE k at time t , and

$$L_0 = 46.3 + 33.9 \log_{10}(f_c) - 13.82 \log_{10}(h_{AP}) - (1.1 \log_{10}(f_c) - 0.7) h_{UE} + (1.56 \log_{10}(f_c) - 0.8), \quad (2)$$

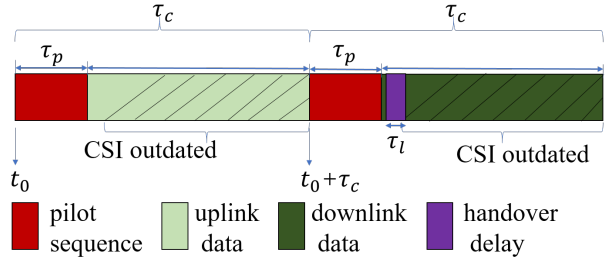


Fig. 2. Illustration of communication blocks of uplink and downlink.

where f_c is the carrier frequency, h_{AP} is the AP antenna height, h_{UE} is the UE antenna height, $d_c = 50$ m, and $d_0 = 10$ m.

The AP-UE channel is assumed to experience Rayleigh fading. The channel between AP m and UE k at time t is modelled as $h_{mk}[t] \sim N_C(0, R_{mk}[t])$, where R_{mk} represents the large-scale fading of the link between AP m and UE k [5], given by $R_{mk}[t] = \beta_{mk}[t]n_0/p_{mk}$. The average signal-to-noise ratio (SNR) of the channel between AP m and UE k is given by $\beta_{mk}[t] = p_{mk}/(L_{mk}[t]n_0)$, where p_{mk} is the transmit power and n_0 is the Gaussian noise between AP m and UE k . The SNR is used to represent the channel quality during serving AP selection and handover decisions, since the throughput performance is correlated with the SNR [9].

We consider a communication block with a total length of τ_c slots and assume the channel measurement and signal processing only happen once per block. As Fig. 2 shows, the uplink and downlink data occupy one block each. We assume a randomly assigned pilot sequence occupying τ_p slots in each communication block and sufficient pilots for each UE to avoid pilot contamination¹. Since the channels are only measured at the beginning of the communication block, channel information is outdated within the block and the channel realizations at different time instants in a block are different due to mobility. We assume the different channel realizations are correlated and the correlation coefficient between the channel realizations at time 0 and time instant t is modelled as the zeroth-order Bessel function of the first kind [9]

$$\rho[t] = J_0 \left[2\pi \frac{v f_c}{c} T_{sa} (t - \tau_p - 1) \right], \quad (3)$$

where v is the speed of the UE, c is the speed of light, T_{sa}

¹Practical handover scheme design also includes pilot assignment under mobility to reduce pilot contamination [17], however this is out of our scope.

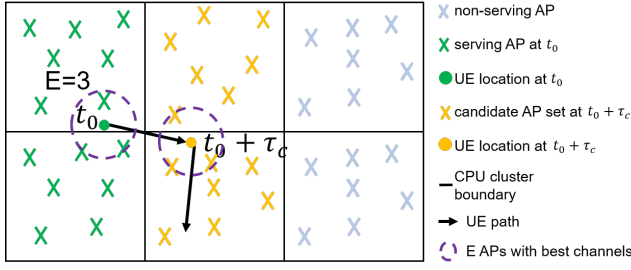


Fig. 3. Illustration of UE mobility for UE-centric CF-mMIMO ($E = 3$).

is the sampling time (i.e., the time for one slot), and τ_p is the length of the pilot sequence. The channel at time t is thus [9]

$$h_{mk}[t] = \rho[t]h_{mk}[0] + \sqrt{1 - \rho^2[t]}g_{mk}[t], \quad (4)$$

where $h_{mk}[0]$ is the channel at time 0, i.e., the initial state, and $g_{mk}[t] \sim N_C(0, R_{mk}[t])$ is the component that is independent of channel aging.

The received signal at AP m for the uplink $y_m^u[t]$ and at UE k for the downlink $y_k^d[t]$ at time t are modelled as

$$y_m^u[t] = \sum_{k=1}^K \sqrt{p_{mk}} h_{mk}[t] x_k + n_0, \quad (5)$$

$$y_k^d[t] = \sum_{m=1}^M \sqrt{p_{mk}} D_{mk}[t] h_{mk}[t] q_{mk} + n_0,$$

where $x_k \sim N_C(0, 1)$ is the transmit signal from UE k and $q_{mk} \sim N_C(0, 1)$ is the transmit signal from AP m intended for UE k . We adopt the dynamic cooperation matrix in [5] to describe the connections between all APs and UEs over the network. We define the $M \times K$ cooperation matrix as D . At time instant t , if there is a connection between AP m and UE k , $D_{mk}[t] = 1$, otherwise $D_{mk}[t] = 0$.

We assume minimum mean-squared error (MMSE) channel estimation $\hat{h}_{mk} \sim N_C(0, Z_{mk}[t])$ [9], where

$$Z_{mk}[t] = \frac{\rho^2 [\tau_p + 1 - t] \beta_{mk}^2[t] n_0}{p_{mk} \sum_{k \in \mathcal{P}_k} \beta_{mk}[t] n_0 + p_{mk}}, \quad (6)$$

with \mathcal{P}_k as the UE set that uses the same pilot as UE k ; (6) thus models the channel aging effect in channel estimation and eventually the throughput performance (*c.f.* Sec. II-D).

When a handover is triggered, a delay τ_l is caused due to the re-forming of the AP-UE link that reduces the throughput by shortening the data transmission time [10]. The handover decision process is detailed in Sec. II-C.

C. Handover in CF-mMIMO

For a mobile UE, the AP serving set is determined every τ_c slots at the beginning of each communication block using Alg. 1. Namely, assuming the starting time is t_0 , the channel measurement and AP serving set updates are triggered at times $t = \{t_0 + n\tau_c\}$, where $n \in \mathbb{N}$ is the number of blocks. Alg. 1 consists of two parts: the first part calculates the candidate AP serving set and the second part is the handover scheme that decides whether to update the serving set to the new candidate set and triggers handovers. We define the average serving set size of all UEs as $G = (\sum_{k=1}^K \sum_{m=1}^M D_{mk}[t]) / K$. The serving AP set for network-centric CF-mMIMO is also determined by Alg. 1 by setting $E = 1$.

Fig. 3 illustrates the mobility of an example UE in UE-centric CF-mMIMO. The UE starts at time instant $t = t_0$

Algorithm 1 Mobile UE-Centric AP Serving Set Determination

Input: The previous SNR $\beta_{mk}[t - \tau_c]$ and the current SNR $\beta_{mk}[t]$ between AP m and UE k for $m = 1, \dots, M$ and $k = 1, \dots, K$. The previous dynamic cooperation matrix $D[t - \tau_c]$. The zero matrix $D'[t] = \mathbf{0}$.

- 1: **for** $k = 1, \dots, K$ **do**
- 2: Sort the APs in descending order based on $\beta_{mk}[t]$, $m = 1, \dots, M$.
- 3: Define the AP index in the descending order as $\{O(1), O(2), \dots, O(M)\}$.
- 4: **for** $e = 1, \dots, E$ **do**
- 5: Define the APs that in the same CPU cluster as AP $O(e)$ as $\mathbf{Q}_{O(e)}$.
- 6: Set $D'_{mk}[t] = 1$, for $m \in \mathbf{Q}_{O(e)}$.
- 7: **end for**
- 8: **end for**
- 9: **switch** handover schemes **do**
- 10: **case** time t is the starting time t_0 or *always-handover*
- 11: Update serving set, set $D[t] = D'[t]$.
- 12: **case** *no-handovers*
- 13: Do not update serving set, set $D[t] = D[t - n\tau_c]$.
- 14: **case** *fairness-differentiated*
- 15: Do Algorithm 2.
- 16: **case** *hysteresis*
- 17: Do Algorithm 3.
- 18: **case** *UE-performance-aware*
- 19: Do Algorithm 4.
- 20: **end switch**

Output: The dynamic cooperation matrix $D[t]$ at time t .

at the position marked with the green dot forms the initial serving AP set with Part 1 in Alg. 1, i.e., Steps 1 - 8. In Steps 1 - 3 of Alg. 1, it finds the E APs with the best channel conditions, i.e., the highest SNR ($E = 3$ in Fig. 3). Then in Steps 4 - 8, the candidate serving set (green crosses) is formed by the APs in the CPU clusters that these E APs belong to [6]. After τ_c slots, the channels are measured and Alg. 1 is triggered again. The candidate AP serving set is calculated based on the new channel measurement at $t = t_0 + \tau_c$. At this time instant, the UE has moved to the yellow dot in Fig. 3 and the candidate serving set (yellow crosses) is different from the current one (green crosses) according to Steps 1 - 8 in Alg. 1. If the candidate set is selected as the new serving set, a handover is triggered, resulting in connection changes of two CPU clusters and $2Q$ APs. However, the actual serving set at $t = t_0 + \tau_c$ might not change to the candidate one if the handover scheme (Part 2, i.e., Steps 9 - 20 in Alg. 1) deems the old serving set to still suffice. We note that the serving set should be updated frequently enough to combat a quickly outdated serving set as the UE location quickly changes. However, overly frequent updates lead to high handover rates and cost. Therefore, a smart handover scheme should be able to reduce the handover rate while still performing necessary serving set updates to achieve high throughput. Part 2 of Alg. 1 considers five different handover schemes (*c.f.* Sec. III).

D. Mobility-Aware Throughput Model

The impact of mobility on the throughput performance is two-fold: channel aging and handover cost [15]. Firstly, we solely consider the channel aging effect and model the baseline throughput performance of the network without handover cost. We use the CF-mMIMO performance model with channel aging in [9] to model the SE of a given UE with handover scheme x as the average spectral efficiency (SE) over a communication block. We then consider the average SE of the uplink and downlink per UE as the *baseline SE performance*,

$$SE_x = \frac{1}{2\tau_c} \sum_{t=\tau_p+1}^{\tau_c} (\log_2(1 + SINR_x^u[t])(1 + SINR_x^d[t])), \quad (7)$$

where $SINR_x^u[t]$ and $SINR_x^d[t]$ are the effective signal-to-interference-and-noise-ratio (SINR) of scheme x at time instant t of the uplink and downlink, respectively, given by [9]

$$SINR_x^u[t] = \frac{S^u}{I^u + n_0}, \quad SINR_x^d[t] = \frac{S^d}{I^d + n_0}, \quad (8)$$

where

$$\begin{aligned} S^u &= \rho^2 [t - \tau_p - 1] \sum_{m=1}^M p_{mk} \left| \omega_{mk}^H[t] D_{mk}[t] \hat{h}_{mk}[t] \right|^2 \\ I^u &= \sum_{k=1}^K \sum_{m=1}^M p_{mk} \left| \omega_{mk}^H[t] D_{mk}[t] \hat{h}_{mk}[t] \right|^2 - S^u \\ S^d &= \rho^2 [t - \tau_p - 1] \sum_{m=1}^M p_{mk} \left| \mathbb{E} \{ h_{mk}^H[t] D_{mk}[t] w_{mk}[t] \} \right|^2 \\ I^d &= \sum_{k=1}^K \mathbb{E} \left\{ \left| \sum_{m=1}^M p_{mk} h_{mk}^H[t] D_{mk}[t] w_{mk}[t] \right|^2 \right\} - S^d \end{aligned} \quad (9)$$

where $\omega_{mk}[t]$ is the combining vector, $w_{mk}[t]$ is the precoding vector for the link between AP m and UE k at time t , and $\hat{h}_{mk}[t]$ is defined by (6). We assume centralized partial MMSE combining and precoding and the vectors $\omega_{mk}[t]$ and $w_{mk}[t]$ are given by (18) in [9]. When $v = 0$ and $\rho[t] = 1$, $Z_{mk}[t]$ in (6) and the baseline SE in (7) are the same as the static performance model in [5].

Secondly, we model the handover overhead as a delay cost. During the handover procedure, the links between the UE and its new serving APs are not yet fully connected and thus cannot perform data transmission. This delay caused by handover reduces the effective throughput by shortening the data transmission time [10]. We consider the SE performance of CF-mMIMO with different handover schemes (*cf.* Sec. III) and model the *mobility-aware* spectral efficiency for handover scheme x as [15]

$$SE_x' = SE_x(1 - d_C H_{C_x} - d_{AP} H_{AP_x}), \quad (10)$$

where SE_x is the baseline SE per UE with channel aging given by (7), d_C is the inter-cluster handover delay, H_{C_x} is the inter-cluster handover rate, d_{AP} is the intra-cluster handover delay, and H_{AP_x} is the intra-cluster handover rate. The handover rate is obtained as the average number of handovers over the mobility period of a single UE. At time instant $t = \{t_0 + n\tau_c\}$, Alg. 1 is triggered and the dynamic cooperation matrix $D[t]$ is updated. The number of handovers

is obtained by comparing $D[t]$ and $D[t - 1]$. We set the number of inter-cluster handovers at time t as the change of connected CPU clusters compared to the serving CPU cluster at $t - \tau_c$. Similarly, the intra-cluster handover is the change of connected APs.

III. FAIRNESS-DIFFERENTIATED HANDOVER SCHEME

A. Fairness-Differentiated: Handover Algorithm Based on Fairness Index

We propose a novel *fairness-differentiated* handover scheme for CF-mMIMO as presented in Alg. 2, which considers the performance trade-off described in (10). To achieve high performance of CF-mMIMO under mobility, i.e., high SE_x' , the handover algorithm should conduct necessary handovers to maintain high baseline throughput under channel aging, i.e., high SE_x . On the other hand, it should also reduce the handover rate by reducing unnecessary handovers, and thus achieve low H_{C_x} and H_{AP_x} . Our algorithm thus differentiates between necessary handovers to be prioritized and optional handovers to be minimized. For the UEs that require urgent handovers, we apply a liberal handover policy to encourage necessary handovers. A strict handover policy is applied to the UEs that do not require urgent handovers to reduce the handover delay cost. We do so by applying different handover policies for the UEs above and below a *handover-policy-differentiation threshold* α obtained via Jain's fairness index, and thus name our handover algorithm *fairness-differentiated*.

In Alg. 2, the UE-specific handover policy is chosen by comparing the UE's total SNR of all serving APs against the threshold that reflects the SNR performance of the whole network, as calculated in Steps 1 - 3. We design the handover-policy-differentiation threshold aiming to preserve the premise of uniform performance for all UEs in CF-mMIMO [2], by enabling good channel conditions from the serving AP set for all UEs. Therefore, we use Jain's fairness index [21] to measure the fairness in terms of the serving AP set channel conditions obtained per UE, given by

$$F = \frac{\left(\sum_{k=1}^K s_k \right)^2}{K \cdot \sum_{k=1}^K s_k^2}, \quad (11)$$

where s_k is the total SNR for UE k of all serving APs at time t , i.e., $s_k = \sum_{m=1}^M \beta_{mk}[t] D_{mk}[t - \tau_c]$. Substituted into (11), we obtain the fairness index for SNR as

$$F = \frac{\left(\sum_{k=1}^K \sum_{m=1}^M \beta_{mk}[t] D_{mk}[t - \tau_c] \right)^2}{K \sum_{k=1}^K \left(\sum_{m=1}^M \beta_{mk}[t] D_{mk}[t - \tau_c] \right)^2}. \quad (12)$$

The fairness index is used to evaluate how fair the quality of the serving AP set of a UE is compared to other UEs in the network, with index values in the range $[1/K, 1]$. The system is considered to be absolutely fair when $F = 1$, where $s_k = 1/K$ for all k , i.e., all UEs obtain the same total SNR, i.e., the same channel conditions. On the other hand, with a low F , the UEs are not fairly served, such that only a few UEs get good channel conditions, i.e., good SNR. Therefore, for KF UEs, the SNR can be considered sufficiently good so that urgent handovers are not required, while the remaining $K(1 - F)$ UEs are considered to be not "fairly served" and

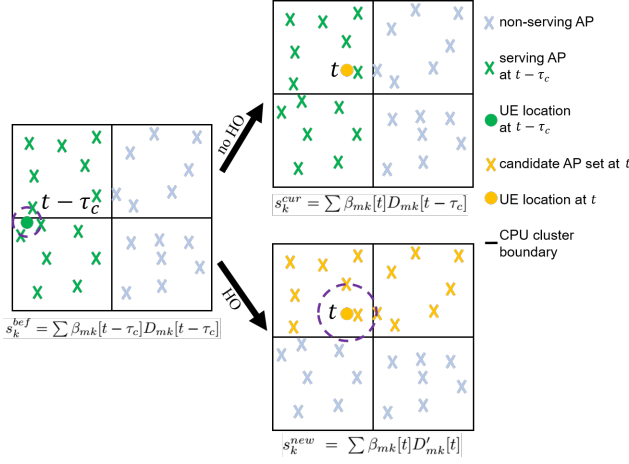


Fig. 4. Illustration of handover decisions at time t (c.f. Steps 4-7 of Alg. 2), showing UE locations, serving AP sets and SNR at different time instants.

would benefit from handovers to switch to better serving sets for a better SNR. According to the fairness index, we set the handover-policy-differentiation threshold α in Steps 2 - 3 of Alg. 2. Next, in Steps 4 - 7, the UE's previous total SNR s_k^{bef} , the UE's current total SNR s_k^{cur} with the connected serving set, and the UE's total SNR with the candidate serving set s_k^{new} are calculated for further comparison. Fig. 4 illustrates the three SNR values. For the example UE, the previous total SNR is obtained with the channel conditions and the selected serving AP set (green crosses) at the previous channel measurement time $t - \tau_c$. The current SNR is provided by this current AP set when the UE moves to the location marked by the yellow dot at the current time t , which is the total SNR at time t if no handover is performed. Following a new channel measurement, the candidate serving AP set (yellow crosses) is then determined by Steps 1 - 8 of Alg. 1. The following steps differentiate the handover policy according to the current SNR of the UE. A UE with a current SNR worse than the threshold α is considered as poorly-served and requires a handover urgently. Therefore, a liberal handover policy is applied in Steps 8 - 14 of Alg. 2, where a handover will be triggered as long as the candidate serving set can provide a better SNR (over a margin γ_1). The other UEs whose SNR is above α are considered well-served and the handover requirement is not urgent. Therefore, a stricter handover policy than in Steps 8 - 14 is applied in Steps 15 - 22. Besides the condition that the candidate serving set should provide better SNR, the UE's current total SNR should also drop below the previous SNR (over a margin γ_2), in order to trigger a handover.

We further consider two handover-triggering conditions of the *fairness-differentiated* scheme in Steps 10 and 17 of Alg. 2, in order to refine the handover policy after separating UEs according to threshold α . We first adopt the same hysteresis handover policy in [18] as handover-triggering Condition A. In this case, the SNR of the candidate serving set s_k^{new} is compared with the previous SNR s_k^{bef} . Alg. 2 can therefore be considered as a modification of the hysteresis algorithm, with hysteresis for UEs above α and a liberal policy for UEs below α . We further design a novel handover-triggering condition, denoted as Condition B, where we compare the SNR of the candidate serving set s_k^{new} to the current SNR

Algorithm 2 Fairness-Differentiated Handover Algorithm Based on Fairness Index

Input: The previous SNR $\beta_{mk}[t - \tau_c]$ and the current SNR $\beta_{mk}[t]$ between AP m and UE k for $m = 1, \dots, M$ and $k = 1, \dots, K$. The previous dynamic cooperation matrix $D[t - \tau_c]$ and the candidate dynamic cooperation matrix $D'[t]$.

- 1: Calculate the Jain's fairness index F with (12).
- 2: Sort the current SNR for all UEs in the ascending order.
- 3: Set the handover policy threshold α as the $((1 - FI)K)^{th}$ value of the current SNR for all UEs
- 4: **for** $k = 1, \dots, K$ **do**
- 5: Calculate the previous total SNR s_k^{bef} for UE k , $s_k^{bef} = \sum \beta_{mk}[t - \tau_c] D_{mk}[t - \tau_c]$, for $m = 1, \dots, M$.
- 6: Calculate the current total SNR without the change of serving set s_k^{cur} for UE k , $s_k^{cur} = \sum \beta_{mk}[t] D_{mk}[t - \tau_c]$, for $m = 1, \dots, M$.
- 7: Calculate the total SNR with the candidate serving set s_k^{new} for UE k , $s_k^{new} = \sum \beta_{mk}[t] D'_{mk}[t]$, for $m = 1, \dots, M$.
- 8: **if** $s_k^{cur} < \alpha$ **then**
- 9: The total SNR of UE k is worse than α .
- 10: **if** (handover-triggering Condition A & $s_k^{new} > s_k^{bef} + \gamma_1$) or (handover-triggering Condition B & $s_k^{new} > s_k^{cur} + \gamma_1$) **then**
- 11: Perform handover, set $D_{mk}[t] = D'_{mk}[t]$, for $m = 1, \dots, M$.
- 12: **else**
- 13: Do not perform handover, set $D_{mk}[t] = D'_{mk}[t - \tau_c]$, for $m = 1, \dots, M$.
- 14: **end if**
- 15: **else**
- 16: The total SNR of UE k is not worse than α .
- 17: **if** (handover-triggering Condition A & $s_k^{new} > s_k^{bef} + \gamma_1$ & $s_k^{cur} < s_k^{bef} - \gamma_2$) or (handover-triggering Condition B & $s_k^{new} > s_k^{cur} + \gamma_1$ & $s_k^{cur} < s_k^{bef} - \gamma_2$) **then**
- 18: Perform handover, set $D_{mk}[t] = D'_{mk}[t]$, for $m = 1, \dots, M$.
- 19: **else**
- 20: Do not perform handover, set $D_{mk}[t] = D'_{mk}[t - \tau_c]$, for $m = 1, \dots, M$.
- 21: **end if**
- 22: **end if**
- 23: **end for**

Output: The dynamic cooperation matrix $D[t]$ at time t .

s_k^{cur} . In this case, the handover will only occur when the candidate serving set achieves better SNR than the current serving set by a certain margin. In Fig. 4, this means that the APs marked by yellow crosses should provide higher SNR than the APs marked by green crosses to the UE at the location marked by the yellow dot. Condition B can thus reduce the unnecessary change of serving AP set when the current set can still provide good performance, e.g., in Fig. 4, the APs marked by green crosses may still provide sufficient SNR to the UE at the location of the yellow dot. We will compare the overall throughput performance of the two handover-triggering conditions in Sec. V-A.

Algorithm 3 Hysteresis Handover Algorithm [18]

Input: The previous SNR $\beta_{mk}[t - \tau_c]$ and the current SNR $\beta_{mk}[t]$ between AP m and UE k for $m = 1, \dots, M$ and $k = 1, \dots, K$. The previous dynamic cooperation matrix $D[t - \tau_c]$ and the candidate dynamic cooperation matrix $D'[t]$.

- 1: **for** $k = 1, \dots, K$ **do**
- 2: Perform Steps 5 to 7 in Algorithm 2
- 3: **if** $s_k^{new} > s_k^{bef} + \delta_1$ and $s_k^{cur} < s_k^{bef} - \delta_2$ **then**
- 4: Perform handover, set $D_{mk}[t] = D'_{mk}[t]$, for $m = 1, \dots, M$.
- 5: **else**
- 6: Do not perform handover, set $D_{mk}[t] = D'_{mk}[t - \tau_c]$, for $m = 1, \dots, M$.
- 7: **end if**
- 8: **end for**

Output: The dynamic cooperation matrix $D[t]$ at time t .

Algorithm 4 UE-Performance-Aware Handover Algorithm [16]

Input: The previous SNR $\beta_{mk}[t - \tau_c]$ and the current SNR $\beta_{mk}[t]$ between AP m and UE k for $m = 1, \dots, M$ and $k = 1, \dots, K$. The previous dynamic cooperation matrix $D[t - \tau_c]$ and the candidate dynamic cooperation matrix $D'[t]$.

- 1: **for** $k = 1, \dots, K$ **do**
- 2: Perform Steps 5 and 6 in Algorithm 2
- 3: **if** $s_k^{cur} < s_k^{bef} - \theta$ **then**
- 4: Perform handover, set $D_{mk}[t] = D'_{mk}[t]$, for $m = 1, \dots, M$.
- 5: **else**
- 6: Do not perform handover, set $D_{mk}[t] = D'_{mk}[t - \tau_c]$, for $m = 1, \dots, M$.
- 7: **end if**
- 8: **end for**

Output: The dynamic cooperation matrix $D[t]$ at time t .

B. Reference Handover Algorithms

We briefly present the reference handover algorithms in this section. The *hysteresis* handover algorithm proposed in [18] is described in Alg. 3. This algorithm monitors the SNR of the individual UE at a given time instant in Step 2 and introduces the hysteresis margins in Steps 3 - 7. Therefore, to trigger a handover, the UE's current SNR must have deteriorated from the previous SNR over a margin δ_1 and the new SNR obtained by the candidate serving set should also be better than the previous SNR over a margin δ_2 . The reference Alg. 3 is thus equivalent to the handover policy for the well-served UE group above the threshold α in our proposed handover scheme with Triggering Condition A (*cf.* Steps 15 - 19 in Alg. 2). The *UE-performance-aware* handover scheme in [16] is described in Alg. 4. The algorithm only compares the UE's previous SNR with the current SNR and triggers handover when the difference exceeds a margin θ .

We note that both Algorithms 3 and 4 only make the handover decisions by comparing the SNR of the UE itself, so that they indiscriminately apply the same handover policy for all UEs in the network. By contrast, our proposed Alg. 2 in Sec. III-A applies a differentiated handover policy to prioritize the handover of UEs that are relatively poorly served, aiming

to achieve uniformly good throughput performance while reducing unnecessary handovers.

In Sec. V, we will compare the throughput performance of our proposed Alg. 2 against the reference Algs. 3 and 4. We will also consider two boundary cases – *always-handover* and *no-handovers* – as references. The *always-handover* scheme is presented in Step 11 of Alg. 1: the UE is always served by the ideal candidate serving set and thus achieves the highest baseline SE as given in (7), but also results in the highest handover rate. By contrast, the *no-handovers* scheme in Step 13 of Alg. 1 does not change the serving set at all during the entire UE mobility path and thus has a handover rate of zero, i.e., $H_C = H_{AP} = 0$, but the lowest baseline SE in (7), due to the most outdated serving set.

C. Computational Complexity of the Handover Schemes

The same channel state measurements, i.e., SNR values β_{mk} between all APs and UEs, are used for both CF-mMIMO combining/precoding [5] and handover decision making for all considered handover schemes in Alg. 2 - 4. Therefore, no additional measurement or signaling overhead is required to perform handover. For the reference *hysteresis* and *UE-performance-aware* handover scheme in Alg. 3 and 4, respectively, no further calculation is required because the handover decision for a UE is only made according to the SNR of the UE itself. Our proposed *fairness-differentiated* scheme does additionally require the calculation of the fairness index in (12) to obtain the threshold α , i.e., Step 1 in Alg. 2. We thus use the computational complexity of (12) to represent the additional complexity of our proposed handover scheme.

To calculate (12), $K \times M$ number of multiplication operations are needed, and thus the computational complexity is of the order of $O(KM)$. Assuming the update of α , i.e., the calculation of (12) is done every b communication blocks, we define the update frequency as $f_{update} = 1/b$. The total computational complexity of α during the mobility period T is then given by

$$C_\alpha = f_{update} \frac{T}{\tau_c} KM. \quad (13)$$

When $f_{update} = 1$, the threshold α is calculated every communication block, resulting in the highest computational complexity for our scheme. By contrast, when $f_{update} \rightarrow 0$, there are nearly no updates of α during the mobility period, leading to a near-zero additional computational complexity of our handover scheme compared to Algs. 3 and 4. We have confirmed via simulations (omitted here for the sake of brevity) that for both a PPP and realistic city network (*c.f.* Sec. IV), the change of α over the period of UE walks is within 2 dB, i.e., a very small change. The SE performance when $f_{update} = 1$ is thus very similar to when $f_{update} \rightarrow 0$. Therefore, our scheme entails a comparable computational complexity as the reference schemes since $C_\alpha \rightarrow 0$.

IV. SIMULATION SCENARIOS

In this section, we present the simulation scenarios and performance metrics used for the evaluation in Sec. V. The corresponding parameters are summarized in Table II.

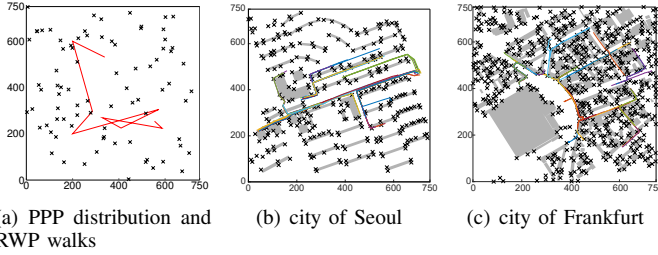


Fig. 5. Network topology with UE walks (APs marked with black crosses and UE mobility pattern marked with colored lines).

We consider a network in an $S = 750 \text{ m} \times 750 \text{ m}$ area. For the AP distribution, we use both PPP and realistic city layouts. For the PPP distribution, we consider $M = 308$ APs randomly uniformly distributed in area S with the density of $\lambda = 547 \text{ AP/km}^2$ corresponding to a medium-density urban network in the city of Seoul, and $M = 665$ ($\lambda = 1182 \text{ AP/km}^2$) corresponding to a high-density urban network in the city of Frankfurt [22]. For the realistic AP distribution, we use publicly available 3D building layouts for the cities [23] and place the APs at all building corners with a height of 10 m to represent a reasonable practical urban deployment [22]. In the PPP networks, we assume $K = 50$ UEs initially distributed according to a PPP distribution with the density of $\lambda_u = 89 \text{ UE/km}^2$ that move according to the RWP model. We assume the UEs move with a fixed speed during each moving period, with a random direction and Rayleigh distributed transition lengths. For the real city layouts, we generate mobility patterns for all K UEs according to specific city topologies with VisWalk [24]. The UEs move along the street, go around buildings, or wait for the traffic lights. The UE movement is thus realistic for a practical urban mobile user but unique to a certain topology of an area. For the medium density network ($\lambda = 547 \text{ AP/km}^2$) and the high density network ($\lambda = 1182 \text{ AP/km}^2$), we assume a cycling speed of 3.6 m/s and a pedestrian speed of 0.8 m/s, respectively, to represent typical urban UE mobility. For all considered scenarios, none of the UEs ever move out of area S and thus the UE density does not change during the entire simulation period. Fig. 5 shows the considered AP distributions and UE walks. Fig. 5(a) shows an example UE walk with the RWP model. The UE makes random turns under no constraints and therefore can go to anywhere in the network. The tracks of all UEs of the two considered cities, Seoul and Frankfurt, are shown in Figs. 5(b) and 5(c) along with the city topologies. We obtain all results as the distribution over all UEs in a network realization, for a UE mobility period of 400 communication blocks and 3200 Monte Carlo network realizations.

We study both UE-centric and network-centric CF-mMIMO architectures (*c.f.* Sec. II-A). For a fair performance comparison, we set the UE-centric architecture to the same average serving AP set size G as the compared network-centric architecture. We first divide area S into $N_c \times N_c$ CPU clusters for the network-centric architecture, leading to $G = Q = M/N_c^2$. We then consider $(N_c + 1) \times (N_c + 1)$ CPU clusters for the compared UE-centric architecture and obtain E via simulation to obtain the same G as the network-centric architecture. For example, in the network with $M = 308$ APs, we divide the

TABLE II
SIMULATION PARAMETERS

Parameter		Value					
handover algorithm		Algs. 2-4					
margin for Alg. 2, $\{\gamma_1, \gamma_2\}$ [dB]		$\{4,4\}, \{1,1\}$					
margin for Alg. 3, $\{\delta_1, \delta_2\}$ [dB]		$\{4,4\}$ [18]					
margin for Alg. 4, θ [dB]		4 [16]					
handover delay, $\{d_C, d_{AP}\}$		$\{0.1 \text{ s}, 0.02 \text{ s}\}$ [25]					
carrier frequency, f_c		2 GHz [9]					
time slot width, T_{sa}		0.1 ms [9]					
$\{\tau_p, \tau_c\}$		$\{10, 200\}$ [9]					
bandwidth		20 MHz [9]					
$\{h_{AP}, h_{UE}\}$		$\{10 \text{ m}, 1 \text{ m}\}$					
$\{K, \lambda_u [\text{UE/km}^2]\}$		$\{50, 89\}$					
UE mobility pattern		RWP realistic walks					
network topology		PPP Seoul			PPP Frankfurt		
$\{M, \lambda [\text{AP/km}^2]\}$		$\{308, 547\}$			$\{665, 1182\}$		
UE speed, [m/s]		3.6			0.8		
network-centric	N_c	3	4	5	3	4	5
	N_c	4	5	6	4	5	6
UE-centric	E	7	4	3	10	7	5
	average serving AP set size, G	34	19	12	73	42	27

area into 3×3 CPU clusters for network-centric CF-mMIMO, leading to an average CPU cluster size $Q = G = 34$. For the UE-centric architecture, we divide the CPU cluster into 4×4 and obtain $E = 7$ via simulation to achieve $G = 34$. The remaining AP selection parameters are listed in Table II.

V. RESULTS

In this section, we evaluate the performance of our *fairness-differentiated* handover scheme for CF-mMIMO proposed in Sec. III-A and compare it against the reference schemes in Sec. III-B under different network architectures and topologies. We first study the basic performance of the proposed scheme in an example PPP network with the UE-centric CF-mMIMO architecture in Sec. V-A. We then extend our performance evaluation to different CF-mMIMO architectures in Sec. V-B. We finally study the performance in different network densities, topologies, and mobility patterns, for both PPP and realistic urban networks in Sec. V-C.

A. Basic Performance of the Fairness-Differentiated Handover Scheme in UE-Centric CF-mMIMO

Let us first consider the PPP distributed network with a density of $\lambda = 547 \text{ AP/km}^2$ and RWP mobility pattern with $v = 3.6 \text{ m/s}$. We set the serving set size $G = 34$ for all considered cases. We will study more AP densities, serving set sizes, network distributions, and UE mobility cases (*c.f.* Table II) in Sec. V-C1. We consider the performance of our proposed scheme with two configurations: handover-triggering Condition A with margins $\gamma_1 = \gamma_2 = 4 \text{ dB}$ as a direct comparison to the reference *hysteresis* scheme with $\delta_1 = \delta_2 = 4 \text{ dB}$ in [18], as well as with Condition B and $\gamma_1 = \gamma_2 = 1 \text{ dB}$ that achieves the best throughput performance for our scheme².

Fig. 6 presents the throughput performance and handover rate of different handover schemes (*c.f.* Sec. III) for the

²We have analysed the performance of our proposed handover scheme via extensive simulations under different handover-triggering conditions A or B, and threshold values i.e., γ_1 and γ_2 over the range of 1-10 dB, and found that Condition B with $\gamma_1 = \gamma_2 = 1 \text{ dB}$ is the best configuration for both UE-centric and network-centric CF-mMIMO architecture among all considered configurations; we omit the full results for the sake of brevity.

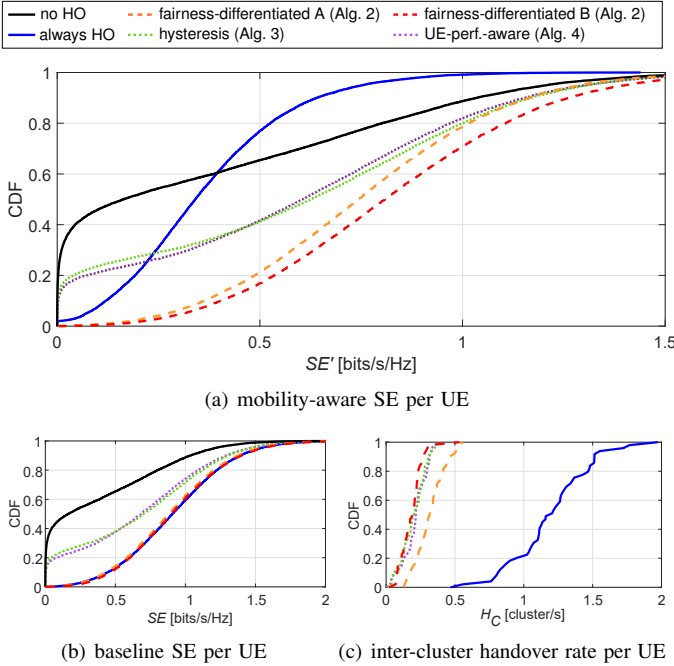


Fig. 6. Throughput performance and handover rate of UE-centric CF-mMIMO with different handover schemes (PPP distribution, RWP mobility, $\lambda = 547$ AP/km², $v = 3.6$ m/s, $G = 34$; $\delta_1 = \delta_2 = 4$ dB for hysteresis, $\theta = 4$ dB for UE-performance-aware, $\gamma_1 = \gamma_2 = 4$ dB for fairness-differentiated with handover-triggering Condition A, and $\gamma_1 = \gamma_2 = 1$ dB for fairness-differentiated with Condition B).

UE-centric CF-mMIMO architecture. Specifically, Fig. 6(a) shows the spectral efficiency SE' given by our throughput model in (10), which considers both the channel aging effect and handover delay cost. In order to examine the impact on the overall throughput performance of these two components, Fig. 6(b) shows the baseline spectral efficiency SE only considering channel aging effect as given in (7), whereas Fig. 6(c) shows the inter-cluster³ handover rate H_C .

Let us start by establishing the basic behavior of UE-centric CF-mMIMO under mobility. Firstly, Figs. 6(a) and 6(b) show that the *no-handovers* reference case suffers severely from outdated AP serving sets, resulting in outage for around 30% of UEs, despite zero handover cost. This indicates that only reducing the handover rate cannot achieve good throughput performance under mobility. Secondly, Fig. 6(a) shows that the *always-handover* case yields significantly better performance for the worst-served UEs compared to the *no-handovers* case, because the UEs are always served by the ideal candidate serving AP set. However, Fig. 6(a) shows that the top 40% of UEs perform significantly worse than with *no-handovers*, despite Fig. 6(b) showing that the *always-handover* case significantly improves the baseline SE for all UEs compared to the *no-handovers* case, since the ideal serving AP set always provides the best channel conditions. Comparing Figs 6(a) and 6(b) thus indicates that for these best-served UEs, frequent handover is unnecessary and the increased handover delay overhead is more harmful for their overall performance than a somewhat stale serving set, highlighting the need for a selective handover scheme. Fig. 6 thus shows that to improve the throughput performance of mobile CF-mMIMO, we cannot

³We focus on the inter-cluster handover since it is the main contributor to the handover cost due to $d_C \gg d_{AP}$ (c.f. Table II).

only consider increasing the baseline SE or reducing the handover rate as prior work [16–19] does. The design of handover schemes of mobile CF-mMIMO should instead strike a balance between preserving the baseline SE performance by encouraging the necessary handover and reducing the handover rate by minimizing unnecessary handovers.

Let us now evaluate the performance of the three considered handover schemes. Fig. 6(a) shows that our proposed *fairness-differentiated* handover scheme with both configurations (i.e. handover-triggering Condition A and B) significantly outperforms the two reference handover schemes and consistently achieves significantly higher throughput under mobility for all UEs compared to the *no-handovers* and *always-handover* case. The superior throughput performance of our proposed handover scheme is, as per its differentiated handover policy design elaborated in Sec. III, due to it performing precise handovers for the UEs “in need”. Figs. 6(b) shows that our proposed handover scheme achieves a comparable baseline SE performance to the *always-handover* case, which is the upper baseline SE bound since the UEs are always served by their ideal AP serving sets. Importantly, our scheme significantly improves the SE of the worst-served UEs compared to the *no-handovers* case, because their handovers are prioritized in our scheme and therefore get timely updates of the serving AP set. Fig. 6(c) shows that our proposed handover scheme reduces the handover rate of UE-centric CF-mMIMO significantly compared to the *always-handover* case due to the selective handover scheme, thus achieving a significant improvement in overall throughput under mobility compared to the *always-handover* case, as Fig. 6(a) shows.

By contrast, the two literature benchmark schemes, *UE-performance-aware* and *hysteresis*, achieve significantly worse throughput performance than our proposed scheme in terms of both SE under mobility (Fig. 6(a)) and baseline SE (Fig. 6(b)). Furthermore, Fig. 6(a) shows that using these prior handover schemes, about 15% of the worst-served UEs remain in outage and about 30% of the worst-served UEs achieve worse performance than the *always-handover* case in SE under mobility. Crucially, this indicates that they fail to trigger necessary handovers for these worst-served UEs due to their indiscriminate handover policy across all UEs, and therefore these worst-served UEs cannot get the chance to improve their performance with a serving set with better channel conditions. Therefore, although Fig. 6(c) shows that these two prior handover schemes may exhibit somewhat lower handover rates than our proposed scheme with Condition A, their performance under mobility is significantly worse than our scheme, as Fig. 6(a) shows. It is worth noting that our proposed scheme does not reduce the handover rate indiscriminately for all UEs like the existing two schemes, but rather assigns necessary handovers to the UEs under the handover policy-differentiated threshold α to update their AP serving set in a timely manner (c.f. Sec. III). In this way, our scheme achieves an improved baseline SE in Fig. 6(b), and thus superior SE under mobility in Fig. 6(a), especially for the worst-served UEs. We emphasize that this is a particularly important result, since the premise of UE-centric CF-mMIMO is to deliver both high and *uniform* throughput results, i.e.,

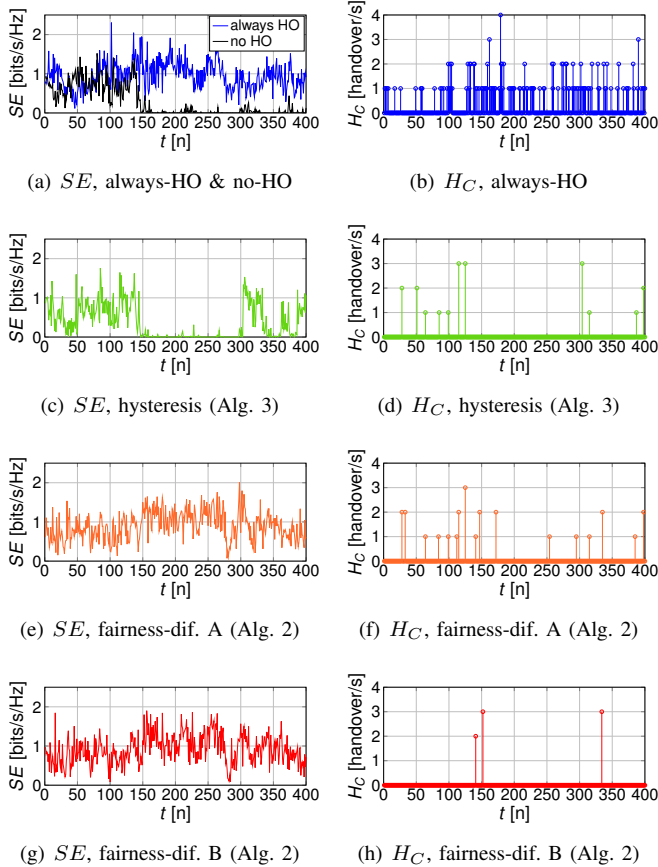


Fig. 7. Baseline spectral efficiency SE and handover rates H_C of an example UE vs. time in UE-centric CF-mMIMO with different handover schemes (PPP distribution, RWP mobility, $\lambda = 547$ AP/km², $v = 3.6$ m/s, $G = 34$; $\delta_1 = \delta_2 = 4$ dB for hysteresis, $\gamma_1 = \gamma_2 = 4$ dB for fairness-differentiated with handover-triggering Condition A, and $\gamma_1 = \gamma_2 = 1$ dB for fairness-differentiated with Condition B).

improving the performance of the poorly-served “edge” UEs.

Furthermore, Fig. 6(a) shows that our scheme with handover-triggering Condition B achieves better throughput performance under mobility than with Condition A, due to the similar baseline SE in Fig. 6(b) but significantly lower handover rate in Fig. 6(c). This is because, according to the definition presented in Sec. III-A, Condition A triggers a handover when the SNR performance of the candidate serving AP set s_k^{new} is better than that of the previously chosen serving set s_k^{bef} by a certain margin. However, if the current serving set can still provide a good SNR to the UE at time t , even better than at time $t - \tau_c$, i.e., $s_k^{cur} > s_k^{bef}$ (c.f. example in Fig. 4), a handover might be unnecessary if the SNR provided by the candidate serving set cannot be higher than s_k^{cur} . By contrast, with Condition B, a handover will only be triggered if the candidate serving set can improve the current SNR performance by a certain margin. Condition B can thus identify a critically outdated serving set more precisely and furthermore reduce the handover rate while maintaining the high baseline SE performance compared to Condition A.

Our proposed *fairness-differentiated* handover scheme is thus designed to not only reduce the handover rate, but also be able to correctly identify the moments when it is necessary to trigger a handover. To directly illustrate this, let us consider an example UE and plot in Fig. 7 the baseline SE and

handover rate of this UE versus time over its mobility path. Fig. 7(a) compares the baseline SE for the *always-handover* and *no-handovers* cases. For the time period $t = 0 - 150n$, the performance with *no-handovers* only degrades a little compared to the *always-handover* case, which means it is unnecessary to conduct so many handovers during this period. At $t = 150n$, the baseline SE with *no-handovers* degrades significantly, which means that handovers must be triggered from this moment to maintain good performance. However, Fig. 7(b) shows that *always-handover* performs frequent handovers over the whole period, regardless of their necessity as revealed by Fig. 7(a). Namely, triggering a handover every time to always maintain the ideal candidate serving set leads to many unnecessary handovers. Fig. 7(d) shows that the *hysteresis* handover scheme in Alg. 3 reduces the handover rate compared to the *always-handover* case shown in Fig. 7(b). However, it does not perform the necessary handover at $t = 150n$, leading to a large throughput degradation as shown in Fig. 7(c). This confirms that the existing handover schemes fail to trigger handovers at the correct moment for the UEs “in-need”, because they treat all UEs indiscriminately. By contrast, Figs. 7(f) and 7(h) show that our proposed handover scheme performs a handover at $t = 150n$, while minimizing handovers at other times. Our scheme thus achieves a comparable baseline SE as the *always-handover* scheme boundary, as shown by comparing Figs. 7(a) and 7(e). This confirms that our proposed *fairness-differentiated* handover scheme is able to perform timely handovers for UEs that need it, while reducing unnecessary handovers for those that do not. Furthermore, comparing Figs. 7(g) to 7(a) and 7(e) shows that our *fairness-differentiated* scheme with both handover-triggering conditions achieves a comparable baseline SE as the *always-handover* upper bound. Importantly, Fig. 7(h) shows that Condition B furthermore lowers the handover rate compared to Condition A in Fig. 7(f), while the necessary handover at time $t = 150n$ is still successfully performed. This confirms that Condition B can more precisely identify the outdated serving set and guarantee performance improvement after handover, by directly comparing the performance of the new candidate serving set to the current (rather than prior, as in Condition A and Alg. 3) performance of the old serving set. We will only consider our *fairness-differentiated* scheme with Condition B and $\gamma_1 = \gamma_2 = 1$ dB in Secs. V-B and V-C, having shown it to be the best performance configuration.

B. Performance of Handover Schemes in Different CF-mMIMO Architectures

In this section we first study the performance of our *fairness-differentiated* scheme and the reference handover schemes with the network-centric CF-mMIMO architecture in Sec. V-B1. We then compare the performance with the UE-centric architecture to study which architecture is preferable in a mobile CF-mMIMO network in Sec. V-B2.

1) *Performance in Network-Centric CF-mMIMO*: Let us now study the mobility performance of the network-centric CF-mMIMO architecture as a comparison to UE-centric CF-mMIMO. We set $Q = G = 34$ for the network-centric architecture and divide the area into 3×3 CPU clusters (c.f. Table

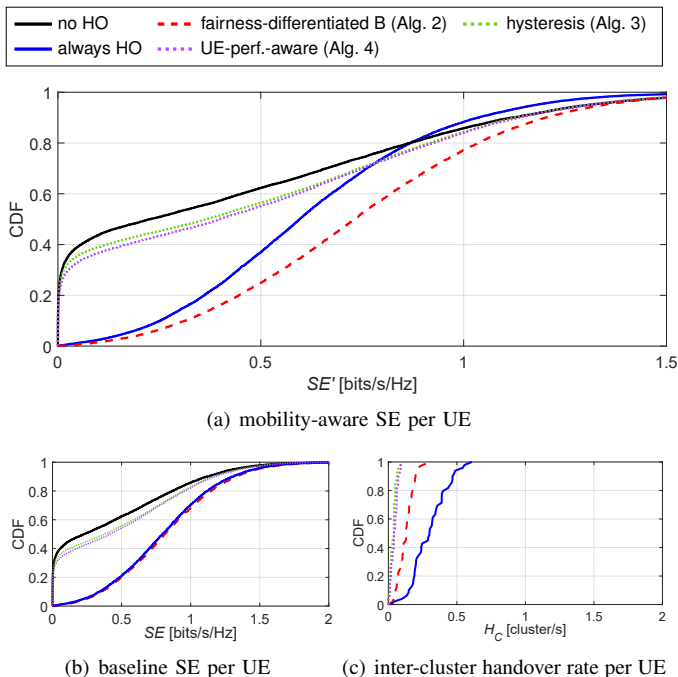


Fig. 8. Throughput performance and handover rate of network-centric MIMO with different handover schemes (PPP distribution, RWP mobility, $\lambda = 547$ AP/km², $v = 3.6$ m/s, $G = 34$; $\delta_1 = \delta_2 = 4$ dB for hysteresis, $\theta = 4$ dB for UE-performance-aware, and $\gamma_1 = \gamma_2 = 1$ dB for fairness-differentiated with handover-triggering Condition B).

II). Fig. 8 shows the throughput performance and handover rate of a network-centric CF-mMIMO network with the same serving AP set size of $G = 34$ as the UE-centric MIMO network in Fig. 6. For the *no-handovers* case, Figs. 8(a) and 8(b) show that for network-centric CF-mMIMO, a similar proportion of the worst-served UEs as for UE-centric in Figs. 6(a) and 6(b) achieve nearly zero throughput. This means that the outdated serving AP set also impacts network-centric CF-mMIMO severely, same as for UE-centric. However, in contrast to the UE-centric network in Fig. 6(a), Fig. 8(a) shows that network-centric MIMO with the *always-handover* case significantly improves the performance of more than 80% of the UEs compared to the *no-handovers* case. Only the top 20% of UEs perform slightly worse than the *no-handovers* case due to frequent unnecessary handovers. Comparing Figs. 8(c) and 6(c) further reveals that, even with the *always-handover* case, the handover rate of network-centric MIMO is significantly lower than that of UE-centric CF-mMIMO. This is because in UE-centric CF-mMIMO, the serving set should always maintain good channel conditions by efficiently “surrounding” the UE. By contrast, network-centric CF-mMIMO only triggers a handover when the UE moves to a different CPU cluster area. This means that the network-centric architecture does not have as many unnecessary handovers as UE-centric CF-mMIMO. Consequently, the two reference handover schemes, *UE-performance-aware* and *hysteresis*, achieve significantly lower throughput performance than the *always-handover* case in both SE under mobility (Fig. 8(a)) and the baseline SE (Fig. 8(b)) even with a very low handover rate shown in Fig. 8(c), because they strictly reduce the handover rate for all UEs and therefore also reduce the baseline SE due to outdated serving AP sets. By contrast, Fig. 8(a)

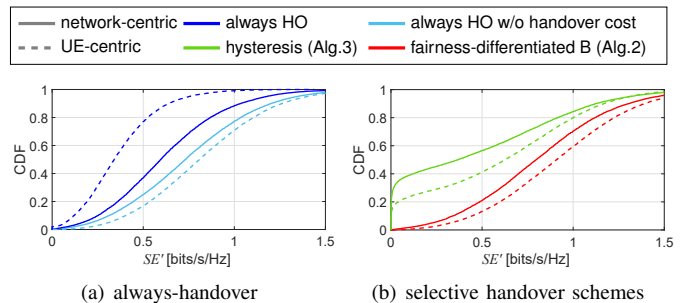


Fig. 9. Spectral efficiency of different network architectures and handover schemes (PPP distribution, RWP mobility, $\lambda = 547$ AP/km², $v = 3.6$ m/s, $G = 34$; $\delta_1 = \delta_2 = 4$ dB for hysteresis and $\gamma_1 = \gamma_2 = 1$ dB for fairness-differentiated with handover-triggering Condition B).

shows that our *fairness-differentiated* handover scheme outperforms all other considered schemes in mobile network-centric CF-mMIMO. Similar to UE-centric CF-mMIMO, Fig. 8(b) shows that our proposed scheme significantly improves the baseline SE compared to the reference cases and achieves very close baseline SE to the *always-handover* upper bound, whereas Fig. 8(c) shows that our scheme obtains a significantly lower handover rate than the *always-handover* case. Studying UE-centric CF-mMIMO and network-centric MIMO separately, we hence show that among all considered handover schemes, our proposed *fairness-differentiated* handover scheme achieves the best performance under the comprehensive mobility-aware throughput model given in (10) for both UE-centric CF-mMIMO and network-centric MIMO architectures. By contrast, the two benchmark schemes from the prior work perform poorly especially for the worst-served UEs, and are therefore unattractive for both architectures.

2) *Performance Comparison of Different CF-mMIMO Architectures*: Let us now directly compare the SE performance of network-centric and UE-centric CF-mMIMO to study which architecture is preferable in a mobile network. Fig. 9 shows the SE under mobility for the two considered network architectures with different handover schemes. Firstly, Fig. 9(a) shows that without considering handover cost, UE-centric CF-mMIMO achieves higher baseline SE than network-centric, as [9] claims. This is because the UE-centric serving AP selection method efficiently surrounds the UE with the serving set (*c.f.* Sec. II-A), and thus reduces the cluster-edge effect compared to the network-centric architecture, where a UE is only served by one CPU cluster. However, Fig. 9(a) also shows that when taking into account handover cost, UE-centric CF-mMIMO with the *always-handover* case achieves a markedly worse SE (i.e., SE' in (10)) than the network-centric architecture, due to its higher handover rate. This confirms that without a smart handover scheme, the UE-centric architecture loses its advantage against network-centric under our comprehensive mobility-aware throughput model, where both channel aging and handover cost are considered. Namely, Fig. 9(a) emphasizes the importance of a selective handover scheme for UE-centric CF-mMIMO to remain attractive.

Next, Fig. 9(b) presents the SE performance for our *fairness-differentiated* handover scheme and the reference *hysteresis* scheme, when both channel aging and handover cost are considered. The *hysteresis* handover scheme exhibits

very similar behavior as *UE-performance-aware*, and thus it is used to represent the considered benchmark schemes in the rest of the paper. With the *hysteresis* scheme, although UE-centric CF-mMIMO achieves higher SE than network-centric for the top 80% of UEs, it remains in outage for the bottom 20% of UEs, due to indiscriminately suppressing handovers. Namely, the *hysteresis* scheme cannot provide sufficient throughput at all for the worst-served UEs, for both UE-centric and network-centric architectures. Therefore, the *hysteresis* scheme fails to preserve the SE improvement for the worst-served UEs in UE-centric CF-mMIMO, which is the key premise of the CF-mMIMO architecture. By contrast, with our *fairness-differentiated* handover scheme, UE-centric CF-mMIMO consistently achieves higher SE for *all* UEs compared to network-centric. Our scheme also consistently achieves higher SE for both architectures compared to *hysteresis*. In summary, Fig. 9 shows that among all considered handover schemes, only our *fairness-differentiated* scheme successfully preserves the SE advantage of UE-centric CF-mMIMO under mobility, making UE-centric again a preferred architecture in mobile networks.

C. Performance in Different Network Configurations

In this section, we study the performance of all considered handover schemes in different network configurations, i.e., network topologies, densities, serving AP set sizes, and UE mobility patterns, to evaluate whether the superior performance of our *fairness-differentiated* handover scheme shown in an example PPP network configuration in Secs. V-A and V-B holds in general.

1) *Performance Under Different PPP Distributed Networks*: In this section, we study the performance of our *fairness-differentiated* handover scheme under different PPP network densities λ and average serving AP set sizes G (c.f. Table II) with the RWP UE mobility pattern. Fig. 10 shows the SE given by (10) of both the median and the worst-performing (95th percentile) UEs and the average handover rate, for all considered PPP networks. Let us first establish the common performance trends for all considered handover schemes. Figs. 10(a)-10(d) show that the SE of all considered scenarios increases with the increase of serving set size G and AP density λ , due to the increase of the desired signal strength (c.f. (9)). Furthermore, the handover rate of all schemes decreases with the increase of G due to the decrease in the number of CPU clusters N_c (c.f. Table II) [10]. We next study the performance of different handover schemes separately. Figs. 10(a)-10(d) show that the SE of the *always-handover* case changes only slightly with G for a given λ for both architectures, due to the highest handover rate among all schemes shown in Figs. 10(e) and 10(f). Furthermore, comparing Figs. 10(a) and 10(c) to Figs. 10(b) and 10(d) shows that the SE of the *always-handover* case of UE-centric CF-mMIMO is always lower than that of network-centric. Importantly, this illustrates that without a selective handover scheme, CF-mMIMO can no longer benefit from a large “surrounding” serving set (i.e. UE-centric with large G) as claimed in [5], due to the high handover cost. The *no-handovers* case achieves the lowest SE among all considered cases despite the zero handover rate and overhead

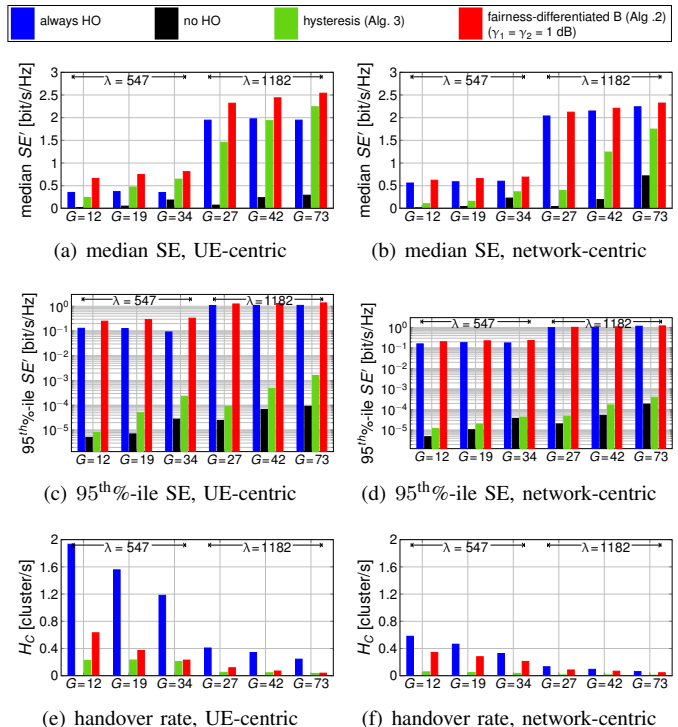


Fig. 10. Mobility-aware spectral efficiency and handover rate of PPP distributed networks, with different CF-mMIMO network architectures, serving set size G , AP density λ [AP/km²], and handover schemes.

due to severely outdated serving AP sets, which emphasizes that solely reducing handover rate cannot achieve high SE under mobility. This also explains why the reference *hysteresis* scheme that indiscriminately suppresses the handovers of all UEs always achieves lower SE in Figs. 10(a)-10(d) than our *fairness-differentiated* handover scheme, despite its lower handover rate in Figs. 10(e) and 10(f).

Figs. 10(a)-10(d) shows that our *fairness-differentiated* handover scheme achieves the best SE among all considered cases. Furthermore, our scheme always achieves higher SE for UE-centric CF-mMIMO than network-centric with the equivalent network configuration (i.e., same G and λ). This demonstrates that our scheme performs well in general for UE-centric CF-mMIMO with PPP distributions. Importantly, Figs. 10(c) and 10(d) show that our scheme achieves significantly higher SE for the worst-performing UEs than *always-handover*, while the *hysteresis* scheme achieves significantly lower SE. This confirms that our scheme is able to in general improve the performance of the worst-performing UEs, by allowing them to perform handover in a timely manner. Overall, Fig. 10 shows that our proposed *fairness-differentiated* handover scheme achieves the best SE performance under mobility among all considered schemes, regardless of G and λ . The advantage of our scheme observed in the example network in Secs. V-A and V-B thus also holds in different PPP network configurations.

2) *Performance in Practical Urban Networks*: Finally, we extend our analysis to realistic urban network topologies and UE mobility patterns in the city area of Seoul (Fig. 5(b)) and Frankfurt (Fig. 5(c)), in order to evaluate the practical performance of our *fairness-differentiated* handover scheme.

Fig. 11 shows the SE and handover rate for the considered urban network cases. Overall, the SE performance trend

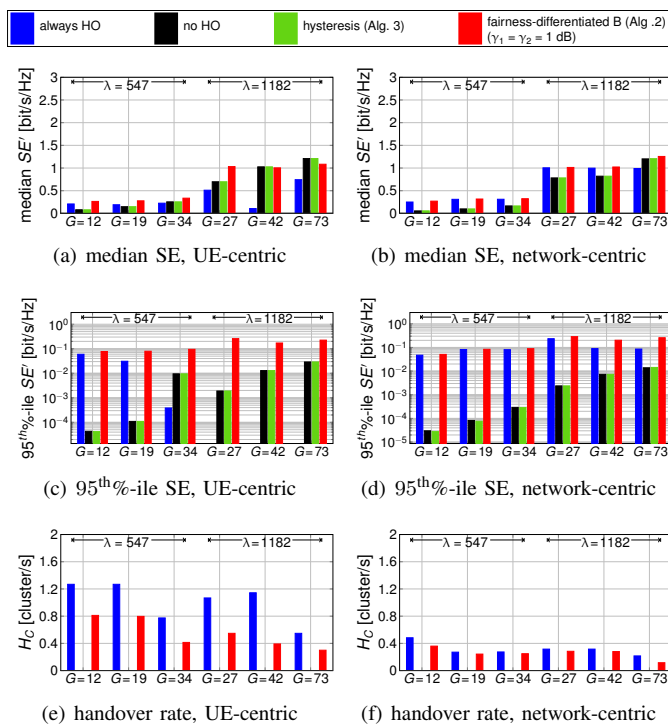


Fig. 11. Mobility-aware spectral efficiency and handover rate of urban networks, with different CF-mMIMO network architectures, serving set size G , AP density λ [AP/km²], and handover schemes.

of different handover schemes is similar to that of PPP distributed networks in Fig. 10. Figs. 11(a)-11(d) show that our *fairness-differentiated* scheme still achieves superior SE in all considered cases, except for UE-centric with $G = 42$ and $G = 73$ in Frankfurt in Fig. 11(a), where the *no-handovers* and *hysteresis* schemes achieve slightly higher median SE performance than our *fairness-differentiated* scheme. This is because, as shown in Fig. 5(c), there are many large building blocks in the area of Frankfurt and the UEs tend to walk around the building, and thus are likely to stay in one CPU cluster during the whole walk, especially when the CPU cluster area is large. In this case, the channel condition change of the serving set is likely to be small during mobility and does not require handover at all for the median-performing UEs. Nonetheless, our scheme achieves a comparable median SE to *no-handovers* and *hysteresis* in these two exceptions, while Fig. 11(c) shows that our scheme achieves orders of magnitude higher SE than the benchmark schemes for the worst-performing UEs. This again highlights that our *fairness-differentiated* scheme especially improves the performance of the worst-performing UEs, and thus fulfills the promise of both high and uniform SE performance of CF-mMIMO in practical networks. Overall, Fig. 11 thus confirms that our proposed *fairness-differentiated* handover scheme is also consistently the best choice in practice, i.e., urban networks with realistic topologies and mobility patterns.

VI. CONCLUSIONS

We studied the performance of mobile CF-mMIMO using a comprehensive throughput model that considers both channel aging and handover cost. We proposed a *fairness-differentiated* handover scheme based on Jain's fairness index that significantly outperforms the existing benchmark handover schemes

for both UE-centric and network-centric CF-mMIMO under mobility. We explicitly compared the performance of different CF-mMIMO architectures and showed that with our handover scheme, UE-centric CF-mMIMO uniquely maintains its throughput advantage against the network-centric architecture under mobility, and thus becomes a feasible architectural concept for not only static but also mobile networks. We furthermore showed that our handover scheme consistently achieves superior throughput for the worst-served UEs compared to the existing schemes in realistic urban network topologies and UE mobility patterns. Importantly, our *fairness-differentiated* handover scheme thus for the first time delivers the original CF-mMIMO promise of uniformly good throughput also in practical mobile networks.

REFERENCES

- [1] Y. Xiao and L. Simić, "A novel socially-differentiated handover scheme for UE-centric cell-free massive MIMO," in *Proc. IEEE WCNC*, Dubai, 2024.
- [2] H. Q. Ngo *et al.*, "Cell-free massive MIMO versus small cells," *IEEE Trans. Wireless Commun.*, vol. 16, no. 3, pp. 1834–1850, 2017.
- [3] E. Björnson *et al.*, *Massive MIMO networks: spectral, energy, and hardware efficiency*, 2017.
- [4] J. Zhang *et al.*, "Cell-free massive MIMO: a new next-generation paradigm," *IEEE Access*, vol. 7, 2019.
- [5] E. Björnson and L. Sanguinetti, "Scalable cell-free massive MIMO systems," *IEEE Trans. Commun.*, vol. 68, no. 7, pp. 4247–4261, 2020.
- [6] G. Interdonato, P. Frenger, and E. G. Larsson, "Scalability aspects of cell-free massive MIMO," in *Proc. IEEE ICC*, Shanghai, 2019.
- [7] R. Irmer *et al.*, "Coordinated multipoint: concepts, performance, and field trial results," *IEEE Commun. Mag.*, vol. 49, no. 2, pp. 102–111, 2011.
- [8] S. Chen *et al.*, "Performance analysis of downlink coordinated multipoint joint transmission in ultra-dense networks," *IEEE Network*, vol. 31, no. 5, pp. 106–114, 2017.
- [9] J. Zheng *et al.*, "Impact of channel aging on cell-free massive MIMO over spatially correlated channels," *IEEE Trans. Wireless Commun.*, vol. 20, no. 10, pp. 6451–6466, 2021.
- [10] Y. Xiao, P. Mähönen, and L. Simić, "Mobility performance analysis of scalable cell-free massive MIMO," in *Proc. IEEE ICC*, Seoul, 2022.
- [11] J. Zheng *et al.*, "Cell-free massive MIMO-OFDM for high-speed train communications," *IEEE J. Sel. Areas Commun.*, vol. 40, no. 10, pp. 2823–2839, 2022.
- [12] K. T. Truong and R. W. Heath, "Effects of channel aging in massive MIMO systems," *J. Commun. Net.*, vol. 15, no. 4, pp. 338–351, 2013.
- [13] W. Jiang and H. D. Schotten, "Impact of channel aging on zero-forcing precoding in cell-free massive MIMO systems," *IEEE Commun. Lett.*, vol. 25, no. 9, pp. 3114–3118, 2021.
- [14] M. Tayyab *et al.*, "A survey on handover management: from LTE to NR," *IEEE Access*, vol. 7, pp. 118907–118930, 2019.
- [15] Y. Xiao and L. Simić, "Mobility performance of scalable cell-free massive MIMO under channel aging and handover," in *Proc. IEEE GLOBECOM*, Kuala Lumpur, 2023.
- [16] R. Beerten *et al.*, "Cell-free massive MIMO in the O-RAN architecture: cluster and handover strategies," in *Proc. IEEE GLOBECOM*, Kuala Lumpur, 2023.
- [17] M. Zaher *et al.*, "Soft handover procedures in mmWave cell-free massive MIMO networks," *IEEE Trans. Wireless Commun.*, vol. 23, no. 6, pp. 6124–6138, 2024.
- [18] R. Karmakar *et al.*, "Mobility management in 5G and beyond: a novel smart handover with adaptive time-to-trigger and hysteresis margin," *IEEE Trans. Mobile Comput.*, pp. 1–16, 2022.
- [19] H. A. Ammar *et al.*, "Handoffs in user-centric cell-free MIMO networks: a POMDP framework," *IEEE Trans. Wireless Commun.*, vol. 23, no. 8, pp. 10319–10335, 2024.
- [20] D. Löschenbrand *et al.*, "Towards cell-free massive MIMO: a measurement-based analysis," *IEEE Access*, vol. 10, 2022.
- [21] J. Deng, Y. S. Han, and B. Liang, "Fairness index based on variational distance," in *Proc. IEEE GLOBECOM*, Honolulu, 2009.
- [22] Y. Xiao, P. Mähönen, and L. Simić, "Poster abstract: Performance of scalable cell-free massive MIMO in practical network topologies," in *Proc. IEEE INFOCOM*, Hoboken, NJ, USA, 2023.

- [23] (2024) OpenStreetMap data extracts. [Online]. Available: <https://download.geofabrik.de/>
- [24] I. Kim, R. Galiza, and L. Ferreira, "Modeling pedestrian queuing using micro-simulation," *Transportation Research Part A: Policy and Practice*, vol. 49, pp. 232–240, 2013.
- [25] W.-Y. Lee and I. F. Akyildiz, "Spectrum-aware mobility management in cognitive radio cellular networks," *IEEE Trans. Mobile Comput.*, vol. 11, no. 4, pp. 529–542, 2012.